

Ab initio electronic structure calculation of correlated systems: EMTO-DMFT approach

L. Chioncel¹, L. Vitos^{2,3}, I. A. Abrikosov⁴, J. Kollár², M. I. Katsnelson^{1,4,5}, and A. I. Lichtenstein¹

¹*University of Nijmegen, NL-6525 ED Nijmegen, The Netherlands*

²*Research Institute for Solid State Physics and Optics, P.O.Box 49, H-1525 Budapest, Hungary*

³*Applied Materials Physics, Department of Materials Science and Engineering, Royal Institute of Technology, SE-10044 Stockholm, Sweden*

⁴*Uppsala University, P.O.Box 530, S-751 21 Uppsala, Sweden*

⁵*Institute of Metal Physics, 620219, Ekaterinburg, Russia*

(10 March 2003)

Abstract

We propose a self-consistent method for electronic structure calculations of correlated systems that combines the local density approximation (LSDA) and the dynamical mean field theory (DMFT). The LSDA part is based on the exact muffin-tin orbitals (EMTO) approach, meanwhile the DMFT uses a perturbation scheme that includes the T -matrix with fluctuation exchange (FLEX) approximation. The current LSDA+DMFT implementation fulfills both self-energy and charge self-consistency requirements. We present results on the electronic structure calculations for bulk 3d transition metals (Cr, Fe and Ni) and for Fe/Cr magnetic multilayers. The latter demonstrates the importance of the correlation effects for the properties of magnetic heterostructures.

I. INTRODUCTION

In the *ab initio* description of the electronic properties of materials the most widely used methods are based on the density functional theory (DFT) [1] implemented within the *local spin density approximation* (LSDA) [2,3] to the exchange and correlation energy. Ground state properties of the most of metals, semiconductors, ionic compounds, etc., are quantitatively well described by the DFT-LSDA approach. Attempts to apply these first principles methods to strongly correlated systems, however, encountered many fundamental difficulties [4–6]. Even for elemental transition metals, such as Mn, Fe, or Ni, the impact of the correlation effects on the electronic structure turns out to be essential [7]. Therefore, one of the most challenging problems in the physics of transition metals, their alloys and compounds is to develop simple and efficient electronic structure methods that go beyond the LSDA by including important many-body effects.

It has proved a fruitful approach to combine the simple Hubbard model with the LSDA technique, providing a DFT scheme "beyond LSDA" [4–7]. Unfortunately, the simplest realization of such an approach, the LSDA+U scheme [4], cannot describe the many-body effects beyond the Hartree-Fock approximation. These effects are connected with the frequency dependence of the electron self-energy. In order to include dynamical effects the LSDA+U scheme was combined with the *dynamical mean field theory* (DMFT) [5,6]. The DMFT maps lattice models onto quantum impurity models subject to a self-consistent condition in such a way that many-body problem for crystal splits into one-body impurity problem for the crystal and many-body problem for an effective atom. In fact, the DMFT, due to numerical and analytical techniques developed to solve the effective impurity problem [8], is a very efficient and extensively used approximation for energy dependent self-energy $\Sigma(\omega)$. The emerged LSDA+DMFT method can be used for calculating a large number of systems with different strength of the electronic correlations [7,9,10]. To underline the importance of complete LSDA+DMFT self-consistency we mention that the first successful attempt to combine the DMFT with LSDA charge self-consistency gave an important insight into a long-standing problem of phase diagram and localization in f-electron systems [11].

To incorporate the dynamical mean field approach in the band structure calculation we adopt the *exact muffin-tin orbitals* (EMTO) density functional method. The EMTO theory can be considered as a screened Korringa-Kohn-Rostoker (KKR) muffin-tin method, where large overlapping potential spheres are used for accurate representation of the LSDA one-electron potential. A comprehensive description of the EMTO theory and its implementation within the LSDA may be found in Refs. [12] and [13,14], respectively.

The paper is organized as follows: Section II presents a general formulation of the combined multiple scattering and dynamical mean field approach. The calculation scheme from Section III illustrates the multiple scattering solution of the LSDA problem via the EMTO method and the many-body solution of the DMFT problem via the T-matrix FLEX approach. First-principles results obtained from EMTO-DMFT calculations are discussed in Section IV. The paper is summarized in Section V.

II. FORMULATION OF THE PROBLEM

The density functional theory reformulates the N electron problem into one electron problem by considering a non-interacting system, where each electron feels an effective potential $v_{eff}^\sigma(\mathbf{r})$ created by the rest of the electrons and external fields. Thus, within the DFT the solution of the original inhomogeneous system is constructed from the one-electron Kohn-Sham equations [2]

$$\left[-\nabla^2 + v_{eff}^\sigma(\mathbf{r})\right] \Psi^\sigma(\epsilon, \mathbf{r}) = \epsilon \Psi^\sigma(\epsilon, \mathbf{r}), \quad (1)$$

where σ stands for spin. The many-body part of the effective potential $\mu_{xc}^\sigma(\mathbf{r})$ is an unknown functional of the spin densities $n^\sigma(\mathbf{r}) = \sum_\epsilon |\Psi^\sigma(\epsilon, \mathbf{r})|^2$. The most commonly adopted approach for $\mu_{xc}^\sigma(\mathbf{r})$ is the *local spin density approximation* (LSDA), where the effect of interactions between electrons is taken into account by substituting locally the real system by the uniform electron gas with the density equal to the actual density at point \mathbf{r} . In this paper we will not distinguish between different specific forms of the LSDA.

In order to include the many-body correlation effects beyond the LSDA we substitute the Kohn-Sham equation (1) by the quasiparticle equation

$$\begin{aligned} & \left[-\nabla^2 + v_{eff}^\sigma(\mathbf{r})\right] \Phi^\sigma(\epsilon, \mathbf{r}) + \\ & + \sum_{Rlmm'} |Rlm\sigma\rangle \Sigma_{Rlm,Rlm'}^\sigma(\epsilon) \langle Rlm'\sigma | \Phi^\sigma(\epsilon) \rangle = \epsilon \Phi^\sigma(\epsilon, \mathbf{r}), \end{aligned} \quad (2)$$

where R, l and m denote the lattice sites, the orbital and the magnetic quantum numbers, respectively. $|Rlm\sigma\rangle$ are localized orthonormal basis functions, e.g. the partial waves for the correlated l -channels. In Eq. (2) the correlation effects are treated at the DMFT level, where the essential many-body self-energy, $\Sigma_{Rlm,Rlm'}^\sigma(\epsilon)$, is a local, energy dependent and multi-orbital potential.

Note that Eqs. (1) and (2) are formulated in terms of wave functions. Consequently, the DMFT method has already been implemented in several techniques based on wave function formalism, like the linear muffin-tin orbital method [5,6,11]. At the same time, accurate self-consistent methods for solving the local Kohn-Sham equation (1) in terms of Green's function have been developed within the multiple scattering theory [15–18]. The main aim of the present work is to include the many-body correlation effects, approximated by means of the DMFT, in the above mentioned multiple scattering approach. We note that for a general non-local energy dependent potential the multiple scattering theory offers a solution known as the optical potential [19]. However, the optical potential is far too complicated to be used in realistic computation. Nevertheless, it is proved that the non-local potential could be transformed into an one particle energy-dependent operator such that it satisfies a similar one-particle equation with local and energy independent potential.

III. THE CALCULATION SCHEME

A. The one-electron Green's function

Within the multiple-scattering formalism, the one-electron Green's function is defined for an arbitrary complex energy z as

$$\left[z + \nabla_{\mathbf{r}}^2 - v_{eff}^{\sigma}(\mathbf{r}) \right] G^{\sigma}(\mathbf{r}, \mathbf{r}', z) = \delta(\mathbf{r} - \mathbf{r}'). \quad (3)$$

For most of the applications, e.g. standard KKR or LMTO methods, the LSDA effective potential from Eq. (3) is approximated by spherical muffin-tin (MT) wells centered at lattice sites R . Within a particular basis set, the one-electron Green's function is expressed in terms of the so-called scattering path operator, $g_{RL,R'L'}^{\sigma,LSDA}(z)$, as well as the regular, $Z_{RL}^{\sigma}(z, \mathbf{r}_R)$, and irregular, $J_{RL}^{\sigma}(z, \mathbf{r}_R)$, solutions to the single site scattering problem for the cell potential at lattice site R , *viz.*

$$\begin{aligned} G^{\sigma,LSDA}(\mathbf{r}_R + \mathbf{R}, \mathbf{r}_{R'} + \mathbf{R}', z) &= \sum_{L,L'} Z_{RL}^{\sigma}(z, \mathbf{r}_R) g_{RL,R'L'}^{\sigma,LSDA}(z) Z_{R'L'}^{\sigma}(z, \mathbf{r}_{R'}) - \\ &- \delta_{RR'} \sum_L J_{RL}^{\sigma}(z, \mathbf{r}_R) Z_{RL}^{\sigma}(z, \mathbf{r}_R), \end{aligned} \quad (4)$$

where $L \equiv (l, m)$ with $l < l_{max}$ (usually $l_{max} = 3$) and $\mathbf{r}_R \equiv \mathbf{r} - \mathbf{R}$ denotes a point around site R . The real space representation for the scattering path operator for the muffin-tin potential is given by

$$g_{RL,R'L'}^{\sigma,LSDA}(z) = [\delta_{RR'} \delta_{LL'} t_{RL}^{\sigma-1}(z) - B_{RL,R'L'}(z)]^{-1}, \quad (5)$$

where $t_{RL}^{\sigma}(z)$ stands for the single scattering t -matrix and $B_{RL,R'L'}(z)$ are the elements of the so-called structure constant matrix.

Unfortunately, the MT based KKR or LMTO methods have limited accuracy. The former method uses non-overlapping spherical muffin-tin potentials and constant potential in the interstitial, while the latter method approximates the system with overlapping atomic sphere and neglects completely the interstitial and the overlap between individual spheres. Recent progress in the field of *muffin-tin orbitals* theory [12] shows that the best possible representation of the full potential in terms of spherical wells may be obtained by using large overlapping muffin-tin wells with exactly treated overlaps. Within this so-called *exact muffin-tin orbitals* method [12], the scattering path operator is calculated as the inverse of the kink matrix defined by

$$K_{RL,R'L'}^{\sigma}(z) \equiv \delta_{RR'} \delta_{LL'} D_{RL}^{\sigma}(z) - S_{RL,R'L'}(z), \quad (6)$$

where $D_{RL}^{\sigma}(z)$ denotes the EMTO logarithmic derivative function [13,14], and $S_{RL,R'L'}(z)$ is the slope matrix [12].

Since the energy derivative of the kink matrix, $\dot{K}_{RL,R'L'}^{\sigma}(z)$, gives the overlap matrix for the EMTO basis set [12], the matrix elements of the properly normalized LSDA Green's function become [13,14]

$$G_{RL,R'L'}^{\sigma,LSDA}(z) = \sum_{R''L''} g_{RL,R''L''}^{\sigma,LSDA}(z) \dot{K}_{R''L'',R'L'}^{\sigma}(z) - \delta_{RR'} \delta_{LL'} I_{RL}^{\sigma}(z), \quad (7)$$

where $I_{RL}^\sigma(z)$ accounts for the unphysical poles of $\dot{K}_{RL,R'L'}^\sigma(z)$. In the case of translation invariance Eqs. (6) and (7) can be transformed to the reciprocal space, so that the lattice index R runs over the atoms in the primitive cell only, and the slope matrix, the kink matrix, and the path operator depend on the Bloch wave vector \mathbf{k} . In this case the total number of states at the Fermi level E_F is obtained as

$$N(E_F) = \frac{1}{2\pi i} \sum_{RL,R'L'} \oint \int_{BZ} G_{RL,R'L'}^{\sigma,\text{LSDA}}(\mathbf{k}, z) d\mathbf{k} dz, \quad (8)$$

where the energy integral includes the Fermi distribution. The \mathbf{k} -integral is performed over the first Brillouin zone, while the z -integral is carried out on a complex contour that cuts the real axis below the bottom of the valence band and at E_F .

B. DMFT Green's function and effective medium Green's function

To incorporate the many-body effects into the Green's function technique we start with the LSDA Green's function matrix (7) expressed on the EMTO basis set. The LSDA+DMFT Green's function, $G_{RL,R'L'}^\sigma(\mathbf{k}, z)$, defined for Bloch vector \mathbf{k} and energy z , is connected to the one-electron LSDA Green's function through the Dyson equation

$$\left[G_{RL,R'L'}^\sigma(\mathbf{k}, z) \right]^{-1} = \left[G_{RL,R'L'}^{\sigma,\text{LSDA}}(\mathbf{k}, z) \right]^{-1} - \delta_{RR'} \tilde{\Sigma}_{RL,RL'}^\sigma(z). \quad (9)$$

The local self-energy $\tilde{\Sigma}_{RL,RL'}^\sigma(z)$ in Eq. (9) depends on the so-called effective medium or *bath* Green's function $\mathcal{G}_{RL,R'L'}^\sigma(z)$. This, in turn, is calculated from the \mathbf{k} -integrated LSDA+DMFT Green's function, $G_{RL,R'L'}^\sigma(z) = \int_{BZ} G_{RL,R'L'}^\sigma(\mathbf{k}, z) d\mathbf{k}$, as

$$\left[\mathcal{G}_{RL,R'L'}^\sigma(z) \right]^{-1} = \left[G_{RL,R'L'}^\sigma(z) \right]^{-1} + \delta_{RR'} \tilde{\Sigma}_{RL,RL'}^\sigma(z). \quad (10)$$

To find the local self-energy we use a *spin polarized T-matrix plus fluctuation exchange* (SPTF) approximation [20]. The many body problem is solved on the Matsubara contour, defined by the fermionic frequencies $\omega_n = (2n + 1)\pi T$, where $n = 0, \pm 1, \dots$, and T is the temperature. A Pade analytical continuation [21] is used to map between the complex energies z , used in the EMTO iterations, and the complex energies $i\omega_n$, corresponding to the Matsubara frequencies and expressed relative to the Fermi level E_F . Next we describe the solution of the effective impurity problem.

C. The solution of effective impurity problem

The many-body problem is solved using the SPTF method proposed in Ref. [20], which is a development of the earlier approach [22]. The SPTF approximation is a multiband spin-polarized generalization of the fluctuation exchange approximation (FLEX) of Bickers and Scalapino, but with a different treatment of particle-hole (PH) and particle-particle (PP) channels. Particle-particle (PP) channel is described by a T -matrix approach [23] giving a renormalization of the effective interaction. This effective interaction is used explicitly in the particle-hole channel. Justifications, further

developments and details of this scheme can be found in Ref. [20]. Here we present the final expressions for the electron self-energy. The sum over the ladder graphs leads to the replacement of the bare electron-electron interaction by the T -matrix which obeys the integral equation

$$\langle 13|T^{\sigma\sigma'}(i\Omega)|24 \rangle = \langle 13|v|24 \rangle - T \sum_{\omega} \sum_{5678} \mathcal{G}_{56}^{i\sigma}(i\omega) \mathcal{G}_{78}^{\sigma'}(i\Omega - i\omega) \langle 68|T^{\sigma\sigma'}(i\Omega)|24 \rangle, \quad (11)$$

where the matrix elements of the screened Coulomb interaction, $\langle 13|v|24 \rangle$, are expressed using the average Coulomb and exchange energies U, J [20]. In this section, for sake of simplicity, we use the short notation $1 = Rlm$. In the following we write the perturbation expansion for the interaction (11). The two contributions to the self-energy are obtained by replacing of the bare interaction by a T -matrix in the Hartree and Fock terms

$$\begin{aligned} \Sigma_{12}^{\sigma, \text{TH}}(i\omega) &= T \sum_{\Omega} \sum_{34\sigma'} \langle 13|T^{\sigma\sigma'}(i\Omega)|24 \rangle \mathcal{G}_{43}^{\sigma'}(i\Omega - i\omega) \\ \Sigma_{12}^{\sigma, \text{TF}}(i\omega) &= -T \sum_{\Omega} \sum_{34\sigma'} \langle 14|T^{\sigma\sigma'}(i\Omega)|32 \rangle \mathcal{G}_{34}^{i\sigma'}(i\Omega - i\omega). \end{aligned} \quad (12)$$

The four matrix elements of the bare longitudinal susceptibility represents the density-density (dd), density-magnetic (dm^0), magnetic-density (m^0d) and magnetic-magnetic channels (m^0m^0). The matrix elements couples longitudinal magnetic fluctuation with density magnetic fluctuation. In this case the particle-hole contribution to the self-energy is written in the Fourier transform form

$$\Sigma_{12}^{\sigma, \text{PH}}(\tau) = \sum_{34\sigma'} W_{1342}^{\sigma\sigma'}(\tau) \mathcal{G}_{34}^{\sigma'}(\tau), \quad (13)$$

τ being the imaginary time. The particle-hole fluctuation potential matrix $W^{\sigma\sigma'}(i\omega)$ is defined in FLEX approximation [24,22]

$$W^{\sigma\sigma'}(i\omega) = \begin{pmatrix} W_{\uparrow\uparrow} & W_{\uparrow\downarrow} \\ W_{\downarrow\uparrow} & W_{\downarrow\downarrow} \end{pmatrix}. \quad (14)$$

We emphasize that all of the above expressions for the self-energy, in the spirit of the DMFT approach, involve the Weiss (bath) Green function (10). The total self-energy is obtained from Eqs. (12) and (13)

$$\Sigma^{\sigma}(i\omega) = \Sigma^{\sigma, \text{TH}}(i\omega) + \Sigma^{\sigma, \text{TF}}(i\omega) + \Sigma^{\sigma, \text{PH}}(i\omega). \quad (15)$$

Since the LSDA Green's function already contains the average electron-electron interaction, in Eqs. (9) and (10) the static part of the self-energy $\Sigma^{\sigma}(0)$, is not included, i.e. we have

$$\tilde{\Sigma}^{\sigma}(i\omega) = \Sigma^{\sigma}(i\omega) - \Sigma^{\sigma}(0). \quad (16)$$

D. The charge self-consistency loop within the EMTO-DMFT scheme

After the self-energy $\tilde{\Sigma}_{RL,RL'}^\sigma(z)$ is determined as the self-consistent solution of the effective impurity problem, the many-body LSDA+DMFT Green's function, $G_{RL,R'L'}^\sigma(\mathbf{k}, z)$, is calculated using Eq. (9). The EMTO-DMFT number of states at the Fermi level is given by the multi center expression (8), written for the LSDA+DMFT Green's function.

The charge and spin densities in the EMTO formalism are represented in one center form around each lattice site R , i.e.

$$n^\sigma(\mathbf{r}) = \sum_{RL} n_{RL}^\sigma(r_R) Y_L(r_R), \quad (17)$$

where $Y_L(r_R)$ are the real harmonics. Inside the Wigner-Seitz cell the partial components $n_{RL}^\sigma(r_R)$ are expressed in terms of the density matrix $\mathcal{D}_{RL'L}^\sigma(z)$ as

$$n_{RL}^\sigma(r_R) = \frac{1}{2\pi i} \oint_{E_F} \sum_{L''L'} C_{L''L'}^L Z_{R''}^\sigma(z, r_R) \mathcal{D}_{RL''L'}^\sigma(z) Z_{R''}^\sigma(z, r_R) dz, \quad (18)$$

where $C_{L''L'}^L$ are the real harmonic Gaunt coefficients. The density matrix is obtained from the path operator as described in, e.g., Ref. [14]. Within the present EMTO-DMFT scheme the LSDA+DMFT path operator, $g_{RL,R'L'}^\sigma(\mathbf{k}, z)$, is determined according to Eq. (7) using the LSDA+DMFT Green's function and the LSDA overlap matrix. Here we implicitly make the assumption that the LSDA+DMFT Green's function can be expanded on the same basis set as the one-electron Green's function. In other words, instead of the solutions of Eq. (2) for a single scatterer, we use the LSDA single-site solutions of Eq. (1) for a single scatterer to express the LSDA+DMFT Green's function in the same form, as we express the one-electron Green's function in Eq. (4).

Finally, for charge self-consistent calculation we construct the new LSDA effective potential from the spin and charge densities, $n(\mathbf{r}) = n^\uparrow(\mathbf{r}) + n^\downarrow(\mathbf{r})$. The Poisson's equation is solved using the spherical cell approximation [14], and the exchange and correlation term is calculated within the LSDA.

IV. RESULTS AND DISCUSSION

The role of the correlation effects in the electronic structure of $3d$ transition metal series is far from being completely understood [7]. In general, spin-polarized band structure calculations give adequate description of the ferromagnetic ground state for the most of metals. At the same time, there are obvious evidences of essentially many-body features in photoemission spectra of Fe [22], Co [25], and Ni [26]. Few examples are the 6 eV satellite in Ni density of states, broadening of the angle-resolved photoelectron spectroscopy (ARPES) features due to quasiparticle damping, narrowing of the d -band, essential change of spin polarization near the Fermi level, etc. Although, there are no direct experimental information yet, one can assume that the many-body effects can also be important in the case of magnetic multilayers and other heterostructures containing transition metals. The importance of correlation effects on transition metal surfaces

has already been demonstrated by the STM observation of an *orbital Kondo resonance* in Cr [27]. Here we will present results obtained using the EMTO-DMFT method in the case of bulk Ni, Fe and Cr *3d* transition metals and for Fe/Cr multilayer structure.

A. Numerical details

The self-consistent EMTO-DMFT calculations were carried out for the experimental ground state crystal structures, i.e. *fcc* for Ni, and *bcc* for Fe and Cr. The lattice parameters were fixed at the experimental values. The studied Fe/Cr multilayer system has *tetragonal* (001) structure with one type of Fe atoms and two different types of Cr atoms. This structural setup describes the situation of one Fe layer embedded in few Cr layers. The atoms in the tetragonal unit cell were fixed in the ideal positions, and for the lattice parameters we used the bulk Cr lattice constant. The LSDA Green's function was calculated for 16 complex energy points distributed exponentially on a semi-circular contour. The k -point sampling was performed on a uniform grid in the Brillouin zone. For the LSDA energy functional we used the Perdew-Wang parametrization [28] of the results by Ceperley and Alder [29]. The DMFT parameters, average Coulomb interaction U , exchange energy J and temperature T , used in the present calculation are listed in the last three columns of Table I.

From the self-consistent density of states (DOS) we have determined the magnetic moment μ and the electronic specific heat coefficient γ . The latter is given by relation

$$\gamma = \pi^2 k_B^2 N(E_F)(1 + \lambda)/3, \quad (19)$$

where $N(E_F)$ is the electronic DOS at the Fermi level, $(1 + \lambda)$ is the mass enhancement factor caused by the electron-phonon interaction. This factor in the case of Ni was estimated to be 1.24 [30]. The present theoretical results for the self-consistent magnetic moments and electronic specific heats, along with the available experimental data are listed in Table I.

B. Ni

It has been shown that the main peculiarities of the experimental Ni photoemission spectra can be understood within the framework of the LSDA+DMFT approach [26]. An exact quantum Monte-Carlo (QMC) solution of the effective impurity problem [26] gives impressive quantitative agreement between the experimental and computational data, both for photoemission spectra and for temperature dependent magnetic properties. Here we will show that the perturbative SPTF approach, employed in the present EMTO-DMFT method, also reproduces the main correlations effects beyond LSDA in Ni, e.g. the narrowing of the band, reduction of the exchange splitting and the appearance of the 6 eV satellite.

The EMTO-DMFT density of states for *fcc* Ni is shown on Fig. 1. For the present choice of the average Coulomb interaction $U = 3eV$, the position of the 6 eV satellite is shifted to the lower energy. This shift and the large broadening of the resonance is due to the perturbative approach of the solver of the effective impurity problem [20].

According to the present result, at $T = 500$ K, i.e. at $T/T_c \approx 0.8$, the reduction of the exchange splitting relative to the LSDA value is 43%. This is in good agreement with 40% estimated from experimental data corresponding to the same temperature. Our results are also in agreement with ARPES measurements [31,32]. The EMTO-DMFT magnetic moment of $0.42\mu_B$, see Table I, represents a reduction of 30% from the LSDA value. This reduction is comparable with 25% evidenced from experimental magnetic moments.

Apart from the many-body self-consistency, the present implementation fulfills also the charge self-consistency. This allows us to monitor the effect of DMFT on the LSDA charge and magnetic moment densities in the real space. Fig. 2 shows the LSDA and LSDA+DMFT magnetic moment densities in Ni along the $\langle 110 \rangle$ direction, which corresponds to the nearest-neighbor distance in the *fcc* unit cell. Comparing the two densities one can interpret the reduction of the magnetic moment in the LSDA+DMFT approach as a slight narrowing of the real space extension of the *d* wave functions.

The energy dependence of the self-energy for Ni, plotted on Fig. 3, near the Fermi level shows the typical Fermi liquid behavior. For the imaginary part we have $-Im \Sigma(E) \propto E^2$, meanwhile the real part of the self-energy has a negative slope $\partial Re \Sigma(E)/\partial E < 0$, where E is the electron energy relative to the Fermi level.

Within the LSDA for the electronic specific heat coefficient we obtain 5.43 mJ/K²mol, which underestimates the experimental value from Ref. [33] by more than 20%. This LSDA value is in good agreement with previous calculations [34,35]. On the other hand, within the LSDA+DMFT approach the electronic specific heat coefficient is 6.78 mJ/K²mol, which reduces the discrepancy between theory and experiment by 19%.

C. Fe

In Fig 4 we compare the LSDA and the LSDA+DMFT density of states for *bcc* Fe. The present LSDA magnetic moment $2.25\mu_B$ is reduced to $2.23\mu_B$ within the LSDA+DMFT approach. We note that our LSDA magnetic moment is in excellent agreement with the one obtained in former *ab initio* calculation [36]. The electronic specific heat coefficient increase from the LSDA value of 2.43 mJ/K²mol to 2.53 mJ/K²mol in the LSDA+DMFT calculation. These values can be compared with the experimental data in the range of 3.11 – 3.69 mJ/K²mol [37]. We can see that in *bcc* Fe the correlation effects are much less pronounced than in *fcc* Ni. This is due to the Fe large spin splitting and the *bcc*-structural dip in the density of states [26]. The energy dependence of the self-energy of Fe, see Fig. 5, corresponds again to the Fermi liquid behavior, similar to the case of Ni.

The *d* band exchange splitting in Fe in the LSDA+DMFT is slightly decreased in comparison with the LSDA result. The temperature dependence of the exchange splitting in Fe was determined by spin-resolved photoemission spectroscopy [38]. The experimental results show a very weak temperature dependence of the exchange splitting in the temperature range $0.3 - 0.85T_c$, where $T_c = 1043$ K. Our calculations for three different temperatures $T/T_c = 0.3, 0.6$ and 0.8 show almost constant *d* band exchange splitting, in perfect agreement with experiment [38] and previous DMFT(QMC)

calculations [7].

D. Cr

The effect of correlations in the case of *bcc* Cr is manifested through a small enhancement of the density of states at the Fermi level, as shown in Fig. 6. The value of electronic specific heat coefficient is 2.88 mJ/K²mol, which represents an improvement of about 40% relative to the LSDA value of 2.07 mJ/K²mol. Our LSDA+DMFT result still underestimates the experimental non-magnetic data of 3.5 mJ/K²mol [39] by 15%. Although, for the bulk Cr the correlation effects are not very important, one can expect strong correlation effects at Cr surfaces, in the light of the observation of essentially many-body phenomenon, the orbital Kondo resonance at Cr(001) surface [27].

To demonstrate the correlation effect on the real space charge distribution in Fig. 7 we have plotted the difference of the LSDA+DMFT and LSDA charge densities in the *bcc* (110) plan. As one can see the main effect of the DMFT charge self-consistency is a redistribution of charge density, suggesting a supplementary accumulation of *d* electrons due to correlation effects inside the muffin-tin spheres and a depletion of density in the interstitial region.

E. Fe/Cr multilayer

In order to test the opportunities of the current LSDA+DMFT approximation further, we have applied this to magnetic heterostructures of alternating magnetic and nonmagnetic layers. The most remarkable property of these systems is the giant magnetoresistance (GMR) measured for a parallel/antiparallel configuration of the magnetic moments belonging to the different layer by application of a magnetic field [40]. Experimentally was found that the magnetic multilayers grown epitaxially shows an enhancement of the electronic contribution to the low temperature specific heat [41]. Standard electronic band structure calculations could not reproduce this enhancement [42], which can be an evidence of the correlation effects. Our aim is to check whether the correlation effects considered in the EMTO-DMFT approach can lead to an essential renormalization of the density of state at the Fermi level $N(E_F)$.

In the LSDA+DMFT calculations for Fe/Cr multilayer we have chosen different values for the average Coulomb interaction and exchange energy for Fe and the two types of Cr atoms. These values are listed in Table I. Although this choice is motivated by the fact that correlation effects for these atoms could be similar in this structure, the present results are more qualitative than quantitative.

The layer resolved LSDA and LSDA+DMFT densities of states for Fe/Cr multilayer are plotted in Fig. 8. Comparing the LSDA and LSDA+DMFT DOS one can see that the correlation effects produce a strong peak at the Fermi level. This can give a qualitative explanation of the heat capacity data discussed above.

The calculated LSDA and LSDA+DMFT magnetic moments are shown in Fig. 9. Our LSDA result is in agreement with previous electronic structure calculations of Fe impurities in a Cr surrounding [43]. We have found that within the LSDA the magnetic

multilayer structure consist of ferromagnetically coupled Fe layers with the magnetic moments of $1.72\mu_B$ per atom. The Cr spacers have very small magnetic moments per atom, $-0.05\mu_B$ and $0.09\mu_B$, respectively, and they are oriented antiferromagnetically. This result is in accordance with previous *ab initio* study on Fe/Cr superlattices [44]. The LSDA Fe magnetic moment is drastically reduced compared with its value in bulk, which is attributed to $d-d$ band hybridization between the Fe and Cr states.

The results of the LSDA+DMFT calculations are essentially different from that in LSDA. In particular, the correlation effects result in a slightly increase of the Fe layer magnetic moment and a significant polarization of the Cr spacers, see Table I. In the case when the correlation effects are considered for all the atoms the selfconsistent calculation shows the same trend for the magnetic moments: $1.85\mu_B$ per Fe atom, $0.42\mu_B$ per Cr1 and $-0.19\mu_B$ per Cr2 respectively. These results leads us to the conclusion that the correlation effects induce a strong polarization on the first Cr layer, which is almost non-magnetic according to the LSDA calculations. The appearance of the Cr magnetic moments can be attributed to the correlation induced narrowing of the d band, together with the Fe-Cr $d-d$ hybridization mechanisms. In the presence of the correlations the Fe-Cr $d-d$ hybridization is much stronger than the Cr₁-Cr₂ $d-d$ hybridization. This can be seen from majority spins channel of DOS from Fig. 8, where Fe d and Cr₁ d have pronounced peaks at the Fermi level. Due to this significant change in the spin up d-channel of DOS of Fe Fig. 8, the spectral weight is transferred close to Fermi level and the effective exchange interaction between the Fe and the first Cr layer is changed becoming ferromagnetic. Further investigation of this magnetic ordering as function of different parameters U, T is important for the nature of the magnetic coupling in multilayer systems.

Several theoretical approaches have been used to explain the magnetic properties of such superlattice structures. Many of these approaches are based on the RKKY-like model [45,46], tight-binding models [47] and, recently, on the results of *ab initio* electronic structure calculations [44]. The magnetic coupling studied in the framework of these models was shown to result from the interplay between the direct $d-d$ hybridization of Fe and Cr atoms and indirect exchange through the sp electrons. The $sp-d$ coupling [44] was found to be reminiscent of the RKKY interaction only for superlattices with more than four Cr layers.

The calculated electronic specific heat coefficients are listed in Table I. The present LSDA+DMFT value of $7.84 \text{ mJ/K}^2\text{mol}$ is in good agreement with recent experimental study [41].

Finally, it is worthwhile to emphasize that the enhanced DOS at the Fermi level, having a many-body correlation origin, can play an important role in the GMR, since this DOS enhancement is strongly spin-dependent. It is more effective for the majority electrons of Fe and Cr₁ (Cr₁ are the one closer to the Fe layer), giving the result of a quasiparticle peak centered at the Fermi level. Our finding is in good agreement with the tendency of the enhancement of electronic contribution to the specific heat in Fe/Cr magnetic multilayers [41].

V. CONCLUSIONS

In this paper we present a LSDA+DMFT scheme on the Exact Muffin-Tin Orbitals basis set. The present EMTO formalism allows us to combine the many body problem with the standard screened KKR(LSDA) method in a self-consistent manner. The many-body self-consistency is reached through self-consistency of self-energy, meanwhile the self-consistent charge density is obtained in the conventional LSDA framework. The results of our EMTO-DMFT calculation are summarized in Table I, and they are in good agreement with former LSDA+DMFT implementations using the LMTO basis set.

Correlations effects in multilayer systems are important for transport properties, giving rise to an enhancement of density of states at the Fermi level. We have studied a simple magnetic multilayer system, and have shown that the effect of correlation is to induce magnetism in non magnetic spacers. We attribute this structure and temperature dependent polarization mechanism to simultaneous: (i) Fe-Cr $d-d$ hybridization and (ii) narrowing of electronic d bands due to many-body correlation effects. We note that the latter mechanism, narrowing of the Cr d band, is significantly stronger than the former one.

ACKNOWLEDGMENTS

L.C. acknowledges the financial supports from: Marie Curie host fellowship Contract Number HPMT-CT-2001-00281, the *Computational Magnetoelectronics* RTN project (HPRN-CT-2000-00143) during his visit in the Research Institute for Solid State Physics and Optics, Budapest, and Kavli Institute for Theoretical Physics through the National Science Foundation Grant No. PHY99-07949. M. I. K. acknowledges the financial support from Russian Science Support Foundation.

This work was supported by the Netherlands Organization for Scientific Research (NWO), grant NWO 047-008-16. The Swedish Natural Science Research Council, the Swedish Foundation for Strategic Research and Royal Swedish Academy of Sciences are acknowledged for financial support. Part of this work was supported by the research project OTKA T035043 of the Hungarian Scientific Research Fund and the Hungarian Academy of Science.

REFERENCES

- [1] P. Hohenberg and W. Kohn, Phys. Rev. **136**, B864 (1964).
- [2] W. Kohn and L. J. Sham, Phys. Rev. **140**, A1133 (1965).
- [3] U. von Barth and L. Hedin, J. Phys. C **5**, 1629 (1972).
- [4] V. I. Anisimov, F. Aryasetiawan, and A. I. Lichtenstein, J. Phys.: Condens. Mat. **9**, 767 (1997).
- [5] V. I. Anisimov, A. I. Poteryaev, M. A. Korotin, A. O. Anokhin, G. Kotliar, J. Phys.: Condens. Matter **9**, 7359 (1997).
- [6] A. I. Lichtenstein and M. I. Katsnelson, Phys. Rev. B **57**, 6884 (1998).
- [7] A. I. Lichtenstein and M. I. Katsnelson, in *Band Ferromagnetism. Ground State and Finite-Temperature Phenomena*, edited by K. Barbeschke, M. Donath, and W. Nolting, Lecture Notes in Physics (Springer-Verlag, Berlin, 2001), p. 75.
- [8] A. Georges, G. Kotliar, W. Krauth, and M. J. Rozenberg, Rev. Mod. Phys. **68**, 13 (1996).
- [9] K. Held, I. A. Nekrasov, G. Keller, V. Eyert, N. Bluemer, A. K. McMahan, R. T. Scalettar, T. Pruschke, V. I. Anisimov, and D. Vollhardt, in *Quantum Simulations of Complex Many-Body Systems: From Theory to Algorithms*, edited by J. Groten-dorst; D. Marx, and A. Muramatsu, NIC Series, vol. 10 (NIC, Juelich, 2002), p. 175.
- [10] G. Kotliar and S. Y. Savrasov, in *New Theoretical Approaches to Strongly Correlated Systems*, edited by A. M. Tsvelik (Kluwer Acad. Publ., Dordrecht, 2001).
- [11] S. Y. Savrasov, G. Kotliar, and E. Abrahams, Nature **410**, 793 (2001).
- [12] O. K. Andersen, O. Jepsen, and G. Krier, in *Lectures on Methods of Electronic Structure calculations*, edited by V. Kumar, O.K. Andersen, and A.Mookerjee (World Scientific Publishing Co., Singapore, 1994), p. 63; O. K. Andersen and T. Saha-Dasgupta, Phys. Rev. B **62**, R16219 (2000).
- [13] L. Vitos, H. L. Skriver, B. Johansson, and J. Kollár, Comp. Mat. Sci. **18**, 24 (2000).
- [14] L. Vitos, Phys. Rev. B **64**, 014107 (2001).
- [15] B. L. Györfy, Phys. Rev. B **5**, 2382 (1972).
- [16] G. Rickayzen, in *Techniques of Physics: Green's functions and condensed matter*, ed. N. H. March (Academic Press, London, 1984).
- [17] J. S. Faulkner and G. M. Stocks, Phys. Rev. B **21**, 3222 (1980)
- [18] P. Weinberger, in *Electron scattering theory for ordered and disordered matter* (Clarendon Press, Oxford, 1990).
- [19] J.R. Taylor, *Scattering Theory: The Quantum Theory of Non-relativistic collision* (Robert E. Krieger Pub. Comp, 1983).
- [20] M. I. Katsnelson and A. I. Lichtenstein, Eur. Phys. J. Phys. B. **30**, 9 (2002).
- [21] H. J. Vidberg and J. W. Serene, J. Low Temp. Phys. **29**, 179 (1977).
- [22] M. I. Katsnelson and A. I. Lichtenstein J. Phys. Condens. Matter **11**, 1037, (1999)
- [23] V. M. Galitski, Zh. Eksper. Teor. Fiz. **34**, 115, 1011 (1958); J. Kanamori, Prog. Theor. Phys **30**, 275, (1963)
- [24] N. E. Bickers and D. J. Scalapino, Ann. Phys. (NY) **193**, 206 (1989).
- [25] S. Monastera, F. Manghi, C. A. Rozzi, C. Arcangeli, E. Wetli, H. J. Neff, T. Greber, J. Osterwalder, Phys. Rev. Lett. **88**, 236402 (2002).

- [26] A. I. Lichtenstein, M. I. Katsnelson, and G. Kotliar, Phys. Rev. Lett. **87**, 067205 (2001).
- [27] O. Y. Kolesnychenko, R. de Kort, M. I. Katsnelson, A. I. Lichtenstein, H. van Kempen Nature **415**, 507 (2002).
- [28] J.P. Perdew and Y. Wang, Phys. Rev. B **45**, 13244, (1992).
- [29] D.M. Ceperley and B.J. Alder, Phys. Rev. Lett. **45**, 566 (1980).
- [30] J. R. Anderson, D. A. Papaconstantopoulos, L. L. Boyer and J. E. Schirber, Phys. Rev. B. **20**, 3172 (1979).
- [31] D. E. Eastman, F. J. Himpsel and J. A. Knapp, Phys. Rev. Lett. **40**, 1514 (1978)
- [32] C.J. Maetz, U. Gerhardt, E. Dietz, A. Ziegler and R. J. Jelitto, Phys. Rev. Lett. **48**, 1686 (1982)
- [33] C. Kittel, *Introduction to Solid State Physics*, 3rd ed. (Wiley, New York , 1966).
- [34] M. M. Steiner, R. C. Albers, L. J. Sham, Phys. Rev. B. **45**, 13272 (1992).
- [35] N. C. Bacalis, N. Theodorakopoulos and D. A. Papaconstantopoulos, Phys. Rev. B. **55**, 11391 (1997).
- [36] D.J. Singh, W. E. Pickett, H. Krakauer, Phys. Rev. B. **43**, 11628 (1991); D. Singh, D. P. Clougherty, J. M. MacLaren, R. C. Albers, C. S. Wang, Phys. Rev. B. **44**, 7701 (1991).
- [37] N. E. Phillips, Crit. Rev. Solid. State Sci. **2**, 467 (1971).
- [38] E. Kisker, K. Schroder, M. Campagna and W. Gudat, Phys. Rev. Lett., **52**, 2285 (1984).
- [39] E. Fawcett, Rev. Mod. Phys. **60**, 209 (1988).
- [40] M.N. Baibich, J.M. Broto, A. Fert, F. Nguyen Van Dau, F. Petroff, P. Etienne, G. Creuzet, A. Friederich, J. Chazelas, Phys. Rev. Lett. **61**, 2472 (1988); G. Binasch, P. Grunberg, F. Saurenbach, W. Zinn, Phys. Rev. B **39**, 4828 (1989).
- [41] B. Revaz, M. -C. Cyrille, B. Zink, Ivan K. Schuller and F. Hellman, Phys. Rev. B **65**, 094417 (2002).
- [42] N. I. Kulikov and C. Demangeat, Phys. Rev. B **55**, 3533 (1997).
- [43] S. Mirbt, I. A. Abrikosov, B. Johansson and H. L. Skriver Phys. Rev. B **55**, 67 (1997).
- [44] K. Ounadjela, C. B. Sommers, A. Fert, D. Stoeffler, F. Gautier and V. L. Moruzzi, Europhys. Lett. **15**, 875 (1991).
- [45] Y. Yafet, J. Appl. Phys. **61**, 4085 (1987).
- [46] Y. Wang, P. M. Levy, and J. L. Fry, J. Magn. & Magn. Mater. **93**, 395 (1991).
- [47] D. Stoeffler and F. Gautier, Prog. Theor. Phys. Suppl. **101**, 139 (1990).

TABLES

	μ_{LSDA} (μ_B)	μ_{DMFT} (μ_B)	γ_{LSDA} (mJ/K ² mol)	γ_{DMFT} (mJ/K ² mol)	$\gamma_{\text{expt.}}$ (mJ/K ² mol)	T (K)	U (eV)	J (eV)
Ni	0.63	0.42	5.43	6.78	7.02 ^a	500	3	0.9
Fe	2.25	2.23	2.43	2.61	3.11,3.69 ^b	325	2	0.9
Cr	-	-	2.07	2.88	3.5 ^c	250	2	0.9
Fe(Fe/Cr)	1.72	1.75					2	0.9
Cr ₁ (Fe/Cr)	-0.05	0.15	6.90*	7.84*	8.7 ± 0.7 ^{*,d}	300	0	0.0
Cr ₂ (Fe/Cr)	0.09	-0.11					0	0.0

^a Ref. [33]

^b Ref. [37]

^c Non-magnetic Cr, Ref. [39].

^d Ref. [41]

* Values corresponding to the magnetic multilayer.

TABLE I. Theoretical magnetic moments, μ , and electronic specific heat coefficients, γ , calculated at LSDA and LSDA+DMFT levels. For comparison some experimental electronic specific heat coefficients are also listed. The experimental values for γ include the enhancement due to electron-phonon coupling, but this enhancement is not included for the calculated band structure values for Fe, Cr and Fe/Cr multilayer. The theoretical γ values for Ni are corrected with $1 + \lambda = 1.24$ according to Eq. (19) and Ref. [30]. In the last three columns the parameters used in the self-consistent EMTO-DMFT calculations are listed.

FIGURES

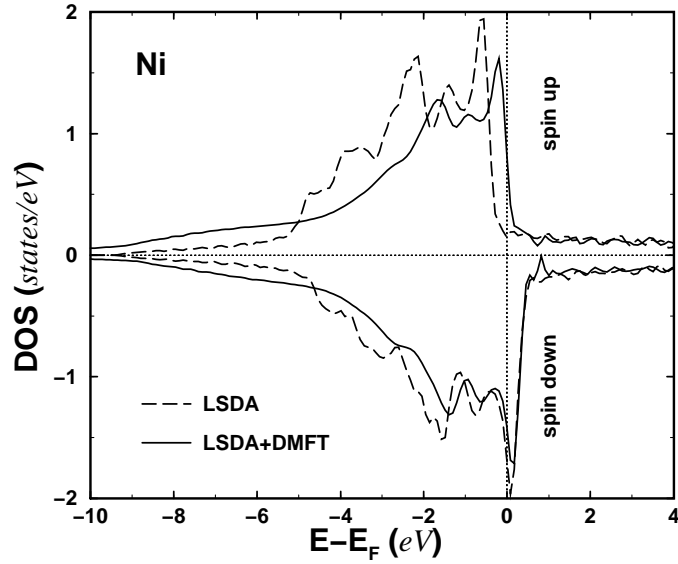


FIG. 1. The LSDA (dashed line) and LSDA+DMFT (solid line) densities of states for *fcc* Ni calculated using the EMTO-DMFT method. A significant reduction of the exchange splitting can be evidenced.

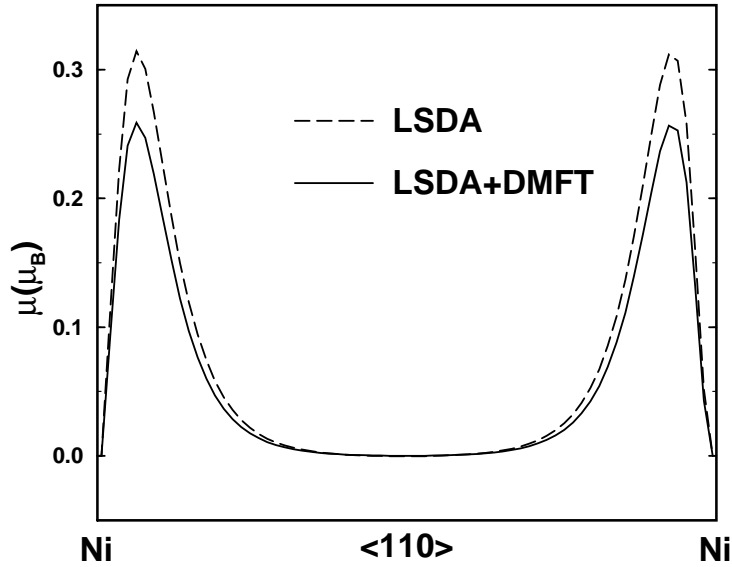


FIG. 2. Magnetic moment densities of Ni along the nearest-neighbor distance in *fcc* lattice, calculated within the LSDA (dashed line) and the LSDA+DMFT (solid line).

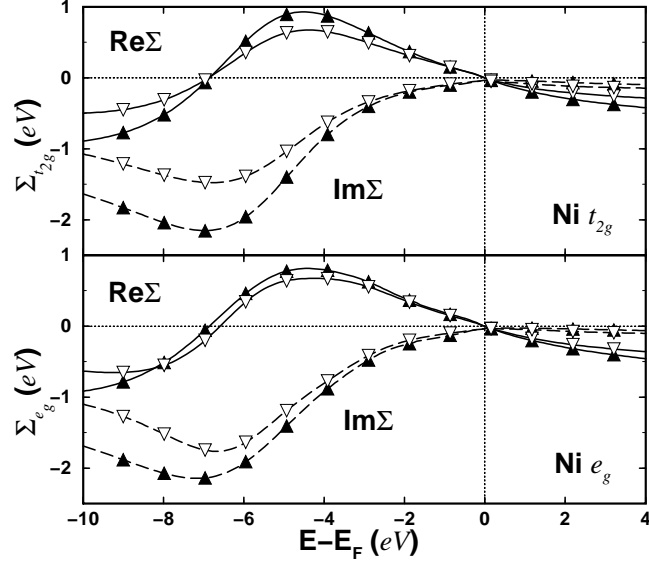


FIG. 3. Spin up (open symbols) and down (closed symbols) self energies for Ni for t_{2g} (upper panel) and e_g (lower panel) orbitals.

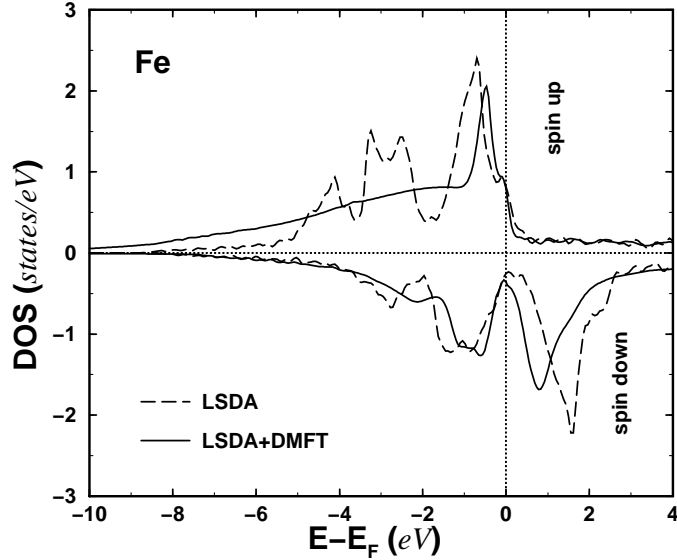


FIG. 4. The LSDA (dashed line) and LSDA+DMFT (solid line) densities of states for bcc Fe calculated using the EMTO-DMFT method.

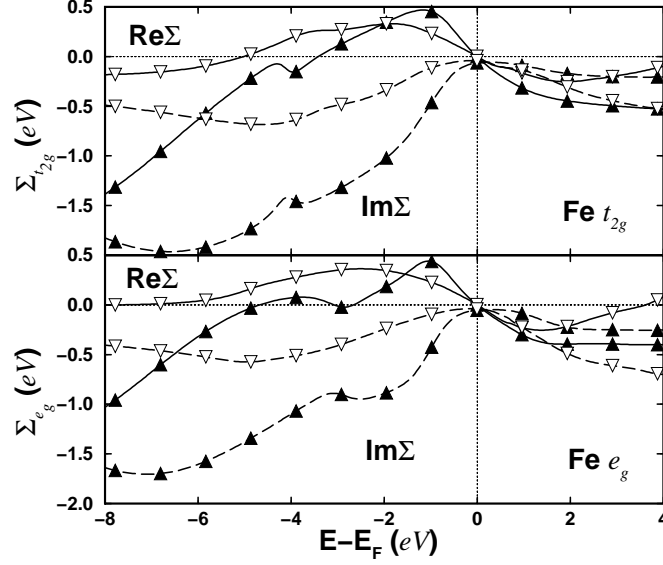


FIG. 5. Spin up (open symbols) and down (closed symbols) self energies for Fe for t_{2g} (upper panel) and e_g (lower panel) orbitals.

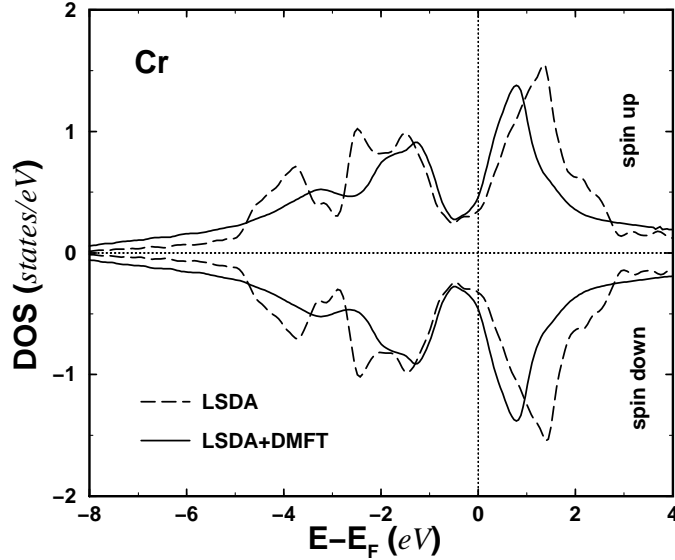


FIG. 6. The LSDA (dashed line) and LSDA+DMFT (solid line) densities of states for *bcc* Cr calculated using the EMTO-DMFT method.

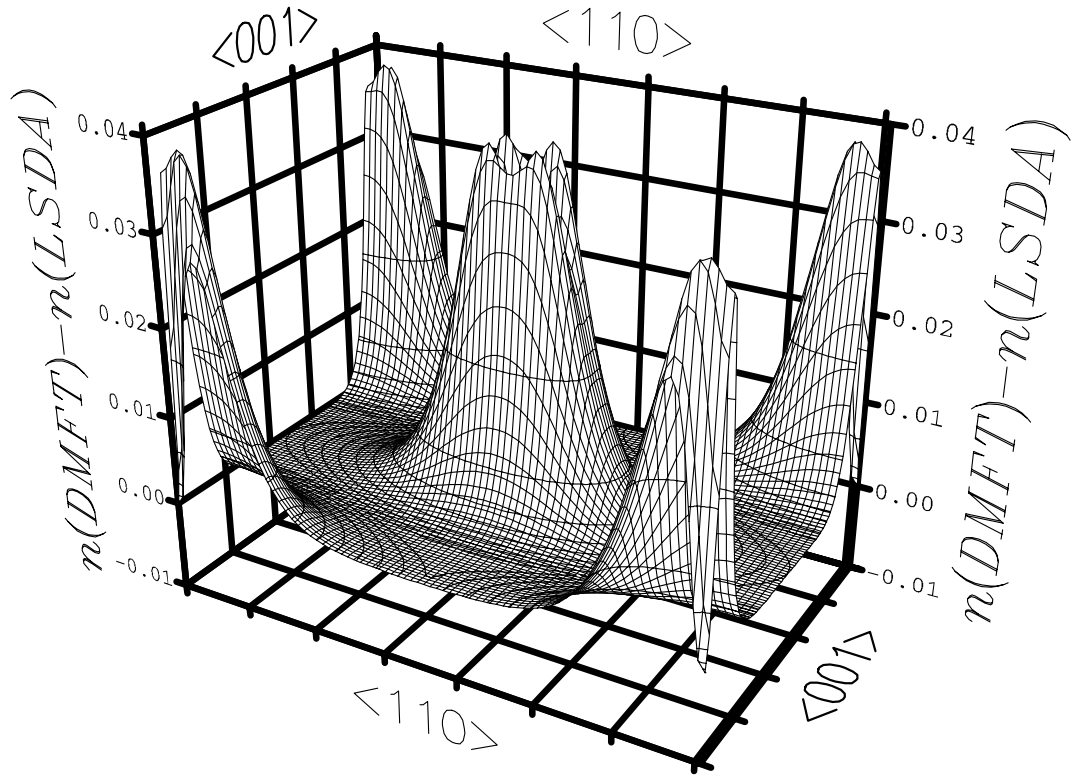


FIG. 7. The effect of DMFT on the LSDA charge density of *bcc* Cr.

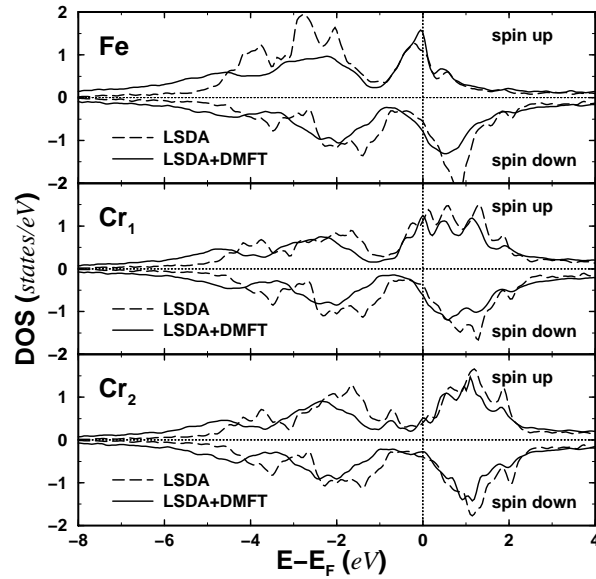


FIG. 8. The layer resolved LSDA (dashed line) and LSDA+DMFT (solid line) densities of states for Fe/Cr₁/Cr₂/Cr₁/Fe multilayers.

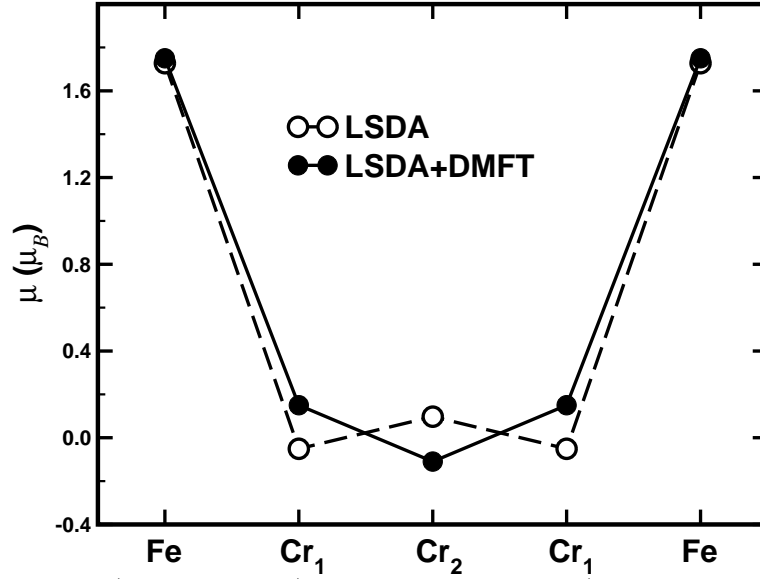


FIG. 9. The LSDA (open symbols) and LSDA+DMFT (closed symbols) magnetic moments per atom for Fe/Cr₁/Cr₂/Cr₁/Fe multilayers.